On the constant stability disk model, MDAR and galaxy scaling relations

Virinchi Rallabhandi
Supervisor: Gerhardt Meurer

Summer 2018/2019

Abstract

My project was born from my supervisor hypothesizing the controversial mass discrepancy acceleration relation (MDAR) could be explained by the constant stability disk model. The model claims a galaxy's gas distribution adjusts to its stellar distribution to maintain a constant value for the Toomre stability parameter, Q. To test the hypothesis, we built a set of "typical" or "template" galaxies built from the model in the hope together, they would trace out the observed MDAR. In short, constant stability is not the enlightening physical insight underlying MDAR. However, we showed it may serve such a purpose in explaining other galaxy scaling relations - namely a correlation between M_{gas}/L_R and V_{max} in HI selected galaxies. As an aside, I realised if MDAR held strictly, as it must in MOND, then the implied dark matter profiles take forms starkly different from those predicted by dark matter simulations. Kinematical studies of real galaxies with highly extended disks could therefore finally settle the debate between MOND and dark matter.

1   Introduction

Throughout my studentship, I've been exploring the constant stability disk model of galaxies. It's a simple, yet effective, galaxy model whose strength comes from its physically motivated description of gas distribution - one of the most disputed galaxy structures. Toomre (1964) provided the first comprehensive analysis regarding the stability of a self-gravitating disk against gravitational collapse. Most usefully, he derived a parameter, Q, whose value at each point in a galaxy is "proportional" to the stability of the disk at that point. The "constant stability disk" or "stable disk" or "constant Q" model assumes Q takes the same value throughout a galaxy. Intuitively, if a region has high star formation activity, the stellar winds and eventual supernovae drive away the surrounding gas hence preventing further star formation via the gas' gravitational collapse. Likewise, if a region has little star formation, the gas can collapse and begin star formation. This negative feedback cycle ensures galaxies' disks maintain stability. Indeed, evidence has built up suggesting Q really is roughly constant within a galaxy (Quirk, 1972; Kennicutt, 1989; Leroy et al., 2008; van der Kruit & Freeman, 2011, among others). In the last few years, a series of papers (Meurer, Zheng & de Blok, 2013; Zheng et al., 2013; Wong et al., 2016) applied the constant Q model with encouraging success in explaining why HI can be used as a tracer of dark matter and predicting star formation rates and efficiencies. Crucially, the stable disk model allows one to inject physical motivation into explaining observed galaxy properties. My project, was to tackle the mass discrepancy acceleration relation (MDAR) with my supervisor's hypothesis that constant Q disks are the physical basis behind MDAR.

Ever since the pioneering efforts of Kapteyn (1922), Zwicky (1937), Rubin (Rubin, Ford & Thonnard, 1980) and many others, the mass discrepancy problem has been an enduring mystery in physics. Wherever we look, be it galaxy clusters or rotation curves, the visible mass is inadequate for reproducing the visible dynamics. Over time, two main solutions have emerged - dark matter and MOdified Newtonian Dynamics (MOND). The former solves the mass discrepancy problem by supposing the existence of vast quantities of matter which emits negligible light, but has a non-negligible gravitational force due to its extent. The latter resolves the issue by adjusting the laws of physics instead. In particular, it claims (Milgrom, 1983)

$$F_g = m\mu(a/a_0)a \tag{1}$$

where F_g is the Newtonian gravitational force, m is the mass of the test particle, a is its acceleration, a_0 is a new fundamental constant and μ is a "MOND interpolating function" which must satisfy $\mu(x) \approx 1$ for $x \gg 1$ and $\mu(x) \approx x$ for $x \ll 1$. Milgrom's genius was realising Newton's laws were never tested on acceleration scales as low

as extragalactic astronomy; we can't assume they still apply. If MOND is correct, the observed accelerations should deviate from those expected from Newton's laws only when $a \ll a_0$. Milgrom (1983) suggests $a_0 = 1.2 \times 10^{-10} m/s^2$ as the most appropriate. Alternatively, from a dark matter point of view, MOND's prediction can still hold true statistically if dark matter only exists in great quantities where accelerations are low. This is the essence of MDAR.

Naturally, astronomers went looking for MDAR; success wasn't elusive (Sanders, 1990; Gentile, Famaey & de Blok, 2011). The most recent and comprehensive update to the MDAR was by McGaugh, Lelli & Schombert (2016) - herafter MLS16. Their extensive sample of 2693 data points from 153 galaxies found almost incontrovertible evidence MDAR exists, at least when averaged across galaxies, with the form

$$g_{obs} = \frac{g_{bar}}{1 - e^{-\sqrt{g_{bar}/g_\dagger}}} \tag{2}$$

where g_{bar} is the radial acceleration due to the the baryons' gravity alone under standard Newtonian mechanics ("baryons" meaning normal, visible matter even though electrons and the like are not baryons), g_{obs} is the observed radial acceleration and $g_\dagger = 1.2 \times 10^{-12} m/s^2$. MLS16 threw down the gauntlet, claiming "the observed coupling between g_{obs} and g_{bar} demands a satisfactory explanation."

It did not take long for responses to come rushing in. Milgrom (2016a) proclaimed a "shot in the arm" for MOND with $g_\dagger = a_0$ and $1 - e^{-\sqrt{g_{bar}/g_\dagger}}$ effectively playing the role of $\mu(a/a_0)$ in equation (1). More challenging, one might imagine, is explaining MDAR in a dark matter dominated universe. There have been several successes in simulations (e.g. see Keller & Wadsley, 2016; Ludlow et al., 2017; Navarro et al., 2017), although their rigour has occasionally been questioned (e.g. by Milgrom, 2016b).

We have a slightly different approach. Rather than trying to model galaxies based on MOND or dark matter tenets, we apply properties we believe to be observationally true - including constant Q. These include long established observational results such as the Tully Fisher Relation (TFR) (Tully & Fisher, 1977), flat rotation curves, mass to light ratios, exponential stellar disks (Freeman, 1970) etc. Therefore any theory explaining existing results, will explain MDAR. Rather than a new law, we aim to show MDAR is a consequence of what we already knew about galaxies. Hence, we build a set of "model" or "template" galaxies from existing observational results and constant Q in the hope that together they will trace out MDAR while highlighting the role of stable disks.

2   Constant stability model

I begin by describing the theoretical and empirical basis underlying our galaxy models. Note that log always refers to base 10; logarithms to base e will always be ln. Furthermore, I've taken the liberty to change variables' notation from the symbols used by the authors who originally defined them. All code required to reproduce the calculations and graphs is available at https://github.com/VirinchiRallabhandi/GalaxyModels (which is perhaps where you found this report anyway).

2.1   How to build a galaxy

There is strong evidence suggesting galaxies' disks are truncated at a particular radius, R_{max}, beyond which the baryonic mass densities fall off abruptly and rapidly (see discussion in Meurer et al., 2018). Ultimately, our model is built upon one independent variable, V_{final}, the rotation speed of objects orbiting the galactic centre at R_{max}. It can be quite challenging to keep track of all the scaling relations we are about to exercise. Hence I include a network of relations employed, figure 1, to assist readers in understanding the way we build a galaxy from V_{final}.

Our galaxy models are essentially a more sophisticated and complete implementation of models by Wong et al. (2016). Our models have two components - a gas disk and a stellar disk. The dark matter is the only "free parameter" and will be dealt with soon (we say "only one free parameter," but one must keep in mind John von Neumann who boasted "with four free parameters I can fit an elephant; with five I can make him wiggle his trunk"). Both disks are truncated at the same radius, R_{max}. Astonishingly, R_{max} happens to be the simplest quantity to deduce. From Meurer et al. (2018),

$$1\,Gy = \frac{2\pi R_{max}}{V_{final}} \implies R_{max} = \frac{V_{final} \times 1\,Gy}{2\pi} \tag{3}$$
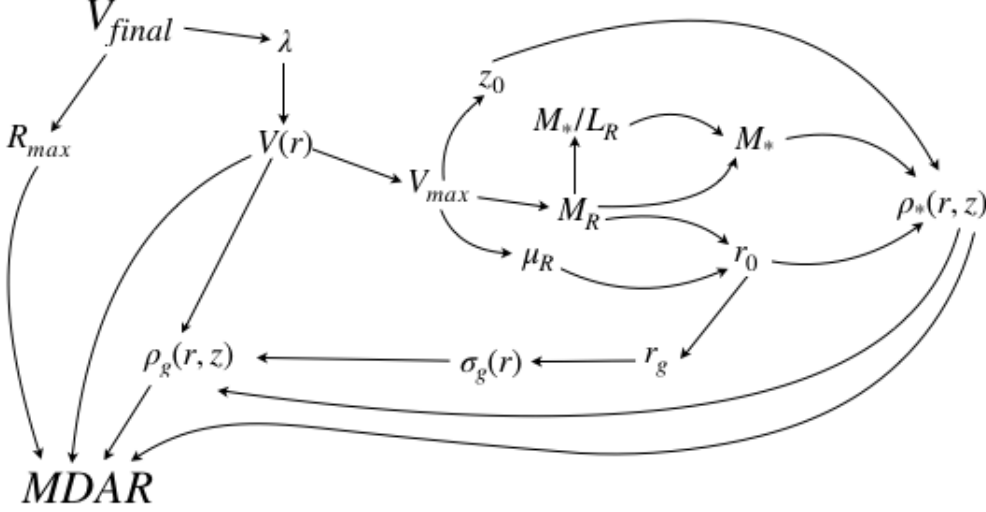
Figure 1: A network of galaxy scaling relations employed to get the MDAR for a galaxy out of our single independent variable, V_{final}. $A \rightarrow B$ means property A is required to deduce property B.

Equally surprisingly, from V_{final} alone, one can deduce the entire rotation curve, $V(r)$. The "universal rotation curve" (URC) of Persic, Salucci & Stel (1996) provides a template which all spiral galaxies should follow. The URC achieves the rare treble of analytic foundation, observational agreement and endurance to time hence being suitable for our purpose. The URC's frankly horrifying form (Persic, Salucci & Stel, 1996; Persic & Salucci, 1991) is

$$V(r)^2 = V_0^2 \left(\frac{1.97a(r/R_{opt})^{1.22}}{(0.61 + (r/R_{opt})^2)^{1.43}} + \frac{b(r/R_{opt})^2}{(r/R_{opt})^2 + c} \right) \tag{4}$$

where

$$a = 0.72 + 0.44 \log \lambda \tag{5}$$

$$b = 1.6e^{-0.4\lambda} \tag{6}$$

$$c = 2.25\lambda^{0.4} \tag{7}$$

$$V_0^2 = \frac{40000\lambda^{0.82}}{0.8 + 0.49 \log \lambda + \frac{0.75e^{-0.4\lambda}}{0.47+2.25\lambda^{0.4}}} \tag{8}$$

$$R_{opt} = 13\sqrt{\lambda} \tag{9}$$

$$\lambda = L/L_* \tag{10}$$

$$L_* = 6 \times 10^{10}/h_{50}^2 \ L_{B\odot} \tag{11}$$

For equation (4) alone, r is in units of kPc, $V(r)$ is in units of km/s and L is the galaxy's luminosity. Hence, all parameters required to deduce $V(r)$ come from L. However, finding L from V_{final} is difficult. Instead, since knowing λ is equally effective, we find the value of λ, by iterative improvement, which gives $V(R_{max}) = V_{final}$.

With $V(r)$, we have sufficient information to find

$$V_{max} = \max_{r \in [0, R_{max}]} V(r) \tag{12}$$

The URC was originally only calibrated for $75 \, km/s \leq V_{max} \leq 300 \, km/s$ which corresponds to $75 \, km/s \leq V_{final} \leq 255 \, km/s$. Hence, our model is restricted to this range.

With V_{max}, a slew of scaling relations are now within our grasp. We assume the stellar component takes the

canonical (Freeman, 1970; van der Kruit & Freeman, 2011) form

$$\rho_*(r, z) = \rho_0 e^{-r/r_0} \operatorname{sech}^2\left(\frac{z}{2z_0}\right) \tag{13}$$

where r_0 and z_0 are the (yet to be determined) "scale length" and "scale height" respectively. van der Kruit & Freeman (2011) find z_0 to simply be

$$z_0 = ((0.45 \pm 0.05)(V_{max}/(100km/s)) - (0.14 \pm 0.07))kPc \tag{14}$$

As we are trying to model a typical galaxy, the scatter/uncertainty may be ignored. Finding r_0 and ρ_0 requires a more scenic route.

Wong et al. (2016) found a number of empirical correlations between R band observations and physical quantities using the Survey for Ionisation in Neutral Gas Galaxies (SINGG) and the Survey for Ultraviolet emission in Neutral Gas Galaxies (SUNGG) data. In particular,

$$M_R = -3.90 - 7.622 \log V_{max} \tag{15}$$
$$\log(M_*/L_R) = -1.578 - 0.0856 M_R \tag{16}$$
$$\log \mu_R = 5.38 + 1.176 \log V_{max} \tag{17}$$

where V_{max} is in km/s, M_R is the galaxy's R band absolute AB magnitude, M_*/L_R is the stellar mass to light ratio in solar units and μ_R is the galaxy's effective surface brightness in $L_\odot/kpc^2$. While most SINGG and SUNGG galaxies reside in the "blue cloud," we can still use these relations as most rotationally supported galaxies form the "blue cloud," rather than "red sequence" anyway. Consequently, using equations (15) - (17), Wong et al. (2016) derive

$$r_0 = \sqrt{\frac{10^{-0.4(M_R - 4.61)}}{5.647\pi\mu_R}} \tag{18}$$

The same equations give us the total stellar mass, M_*, by

$$M_* = L_R 10^{-1.578 - 0.0856 M_R} \tag{19}$$
$$= 10^{-0.4(M_R - 4.61)} \times 10^{-1.578 - 0.0856 M_R} \tag{20}$$

However,

$$M_* = \int_{-\infty}^{\infty} \int_0^{\infty} 2\pi r \rho_*(r, z)\, dr dz \tag{21}$$

$$= 4\pi \int_0^{\infty} \int_0^{\infty} \rho_0 r e^{-r/r_0} \operatorname{sech}^2\left(\frac{z}{2z_0}\right) dr dz \tag{22}$$

$$= 8\pi \rho_0 z_0 r_0^2 \tag{23}$$

using standard integration techniques.

$$\therefore \rho_0 = \frac{M_*}{8\pi z_0 r_0^2} \tag{24}$$

and hence the stellar mass distribution is determined.

We apply the constant Q disk model to determine the gas distribution, $\rho_g(r, z)$. Toomre (1964), found the stability of a disk at a given point, its propensity to resist gravitational collapse there, is "proportional" to his stability parameter

$$Q = \frac{\sigma\kappa}{\pi G \Sigma} \tag{25}$$

where, at a particular point, σ is the material's velocity dispersion, Σ is the material's surface mass density and κ is the epicycle frequency defined as

$$\kappa(r) = \frac{V(r)}{r}\sqrt{2\left(1 + \frac{r}{V(r)}\frac{dV(r)}{dr}\right)} \tag{26}$$

4

For a cylindrically symmetric volume mass density, $\rho(r, z)$, the appropriate definition of surface mass density is

$$\Sigma(r) = \int_{-\infty}^{\infty} \rho(r, z) \, dz = 2 \int_{0}^{\infty} \rho(r, z) \, dz \tag{27}$$

While Toomre (1964) considered disks made from a single material, our galaxy models have two interacting components - stars and gas. We require an expression of Q which accommodates our model's complexity. Zheng et al. (2013) tried various prescriptions for a "two fluid" (two material) stability parameter, Q_{2f}. The prescription closest to the elusive combination of simplicity and accuracy is by Wang & Silk (1994), who derived

$$\frac{1}{Q_{2f}} = \frac{\pi G \Sigma_g}{\sigma_g \kappa} + \frac{\pi G \Sigma_*}{\sigma_{*,r} \kappa} \tag{28}$$

where σ_g is the gas' velocity dispersion, $\sigma_{*,r}$ is the stars' radial velocity dispersion and Σ_g and Σ_* are the surface mass densities of the gas and stars respectively.

$$\therefore \Sigma_g = \frac{\sigma_g \kappa}{\pi G Q_{2f}} - \frac{\sigma_g \Sigma_*}{\sigma_{*,r}} \tag{29}$$

We can in fact derive all the terms on the right hand side. Note that stars are assumed collisionless hence allowing different velocity dispersions in different directions. Gas however, must have the same velocity dispersion in each direction.

$$\Sigma_*(r) = \int_{-\infty}^{\infty} \rho_*(r, z) \, dz \tag{30}$$

$$= 2 \int_{0}^{\infty} \rho_0 e^{-r/r_0} \operatorname{sech}^2 \left(\frac{z}{2z_0} \right) dz \tag{31}$$

$$= 4 z_0 \rho_0 e^{-r/r_0} \tag{32}$$

σ_g is typically assumed to be a constant (Zheng et al., 2013; Leroy et al., 2008), but in reality this isn't the case (O'Brien, Freeman & van der Kruit, 2010; Ianjamasimanana et al., 2015). The most recent and comprehensive analysis by Ianjamasimanana et al. (2015) finds

$$\sigma_g(r) = \sigma_0 e^{-r/r_g} \tag{33}$$

with $r_g = 3.7 r_{25}$. However for Ianjamasimanana et al. (2015)'s sample, there is a very strong correlation between r_0 and r_{25}. Re-analysing their sample, I found

$$r_{25} = (4.426 r_0 / kPc - 0.5507) \, kPc \tag{34}$$

with a correlation coefficient of 0.91486.

$$\therefore r_g = 3.7(4.426 r_0 / kPc - 0.5507) \, kPc \tag{35}$$

is equally valid. Ianjamasimanana et al. (2015) also find the mean gas velocity dispersion to be $8 \, km/s$ regardless of morphology.

$$\therefore 8 \, km/s = \frac{1}{R_{max}} \int_{0}^{R_{max}} \sigma_0 e^{-r/r_g} \, dr \tag{36}$$

$$= \frac{\sigma_0 r_g (1 - e^{-R_{max}/r_g})}{R_{max}} \tag{37}$$

$$\therefore \sigma_0 = \frac{R_{max} \times 8 \, km/s}{r_g (1 - e^{-R_{max}/r_g})} \tag{38}$$

Here I've weighted each radius equally in equation (36). Alternatively, I could weight outer radii higher than inner radii because there's greater area in a ring of radius dr at higher radii. It was unclear to me from Ianjamasimanana et al. (2015) which was more appropriate and I essentially made an arbitrary choice. For $\sigma_{*,r}$, we adopt the approach of Zheng et al. (2013) and Leroy et al. (2008) who find a "typical" velocity dispersion ellipsoid has

$$\sigma_{*,r} = 1.67 \sigma_{*,z} \tag{39}$$

for which van der Kruit & Freeman (2011) derive

$$\sigma_{*,z}(r) = \sqrt{2\pi G \Sigma_*(r) z_0} \tag{40}$$

$$= 2z_0 \sqrt{2\pi G \rho_0 e^{-r/r_0}} \tag{41}$$

We're left with the matter of Q_{2f}. Our fundamental gas distribution proposition is constant Q_{2f}. But which constant? As aforementioned, many scientists observe a constant Q in their galaxies, but unfortunately they do not report the same value; $Q2f$ varies between at least 1.5 and 2.5 across samples (van der Kruit & Freeman, 2011). For our model, we've taken the average value, $Q_{2f} = 2$. While this may be somewhat unsatisfactory, there may be some physical justification from $Q_{2f} = 2$ from figure 21 and discussion in section 7.

Therefore, we now have all the ingredients to find Σ_g via equation (29). Next, we must translate the 2D surface mass density, $\Sigma_g(r)$, into a 3D volume mass density, $\rho_g(r,z)$. van der Kruit (1981) showed a gas disk responding to a stellar disk's force field must maintain

$$\rho_g(r,z) = \rho_g(r,0) \operatorname{sech}^{2p}\left(\frac{z}{z_g}\right) \tag{42}$$

where z_g is the gas disk's scale height and

$$p = \frac{\sigma_{*,z}^2}{\sigma_{g,z}^2} \tag{43}$$

the ratio of the stellar and gas velocity dispersions in the z direction squared. Unlike z_0, z_g varies radially. van der Kruit (1981) finds to within 3% accuracy,

$$W(r) = \frac{1.7\sigma_{g,z}}{\sqrt{2\pi G p \rho_*(r,0)}} \tag{44}$$

where $W(r)$ is the disk's full width at half maximum at radius r and $\sigma_{g,z} = \sigma_g/\sqrt{3}$ as the gas' velocity dispersion is the same in all directions. Furthermore, due to the exponential decline in $\rho_*(r,0)$,

$$W(r) \propto e^{r/2r_0} \tag{45}$$

i.e. the gas disk flares. Unfortunately, equation (44) requires $p \geq 1 \iff \sigma_{*,z} \geq \sigma_{g,z}$, which cannot be ensured as $\sigma_{*,z} \propto e^{-r/2r_0}$ by equation (41). It seems van der Kruit (1981) doesn't really consider $p < 1$ to be possible and we thought it may make sense for the stellar velocity dispersion to be maintained by the gas velocity dispersion. Therefore, since $2r_0 < r_g$ and hence the stellar velocity dispersion falls faster than the gas velocity dispersion, we adjust equations (41) and (39) minimally to

$$\sigma_{*,z}(r) = 2z_0\sqrt{2\pi G \rho_0 e^{-r/r_0}} + \sigma_{g,z}(R_{max}) \tag{46}$$

$$\sigma_{*,r}(r) = 1.67 \times 2z_0\sqrt{2\pi G \rho_0 e^{-r/r_0}} + \sigma_{g,z}(R_{max}) \tag{47}$$

hence ensuring $p \geq 1$. Now with equations (44) and (42) we get

$$\frac{1}{2} = \operatorname{sech}^{2p}\left(\frac{W}{2z_g}\right) \tag{48}$$

which is a quadratic in $e^{W/2z_g}$ and can be solved to get

$$z_g(r) = \frac{W(r)}{2\ln\left(2^{1/2p} + \sqrt{2^{1/p} - 1}\right)} \tag{49}$$

which leaves only $\rho_g(r,0)$ to get in equation (42). From equations (29) and (27) we get

$$\rho_g(r,0) = \frac{\Sigma_g(r)}{2z_g \int_0^\infty \operatorname{sech}^{2p}(x)\, dx} \tag{50}$$

The integral can be evaluated explicitly in terms of hypergeometric function, $_2F_1$, but simpler, numerical methods work equally well.

Having now fully determined $\rho_*(r,z)$, $\rho_g(r,z)$ and $V(r)$, we can deal with dark matter. Dark matter is essentially the one "free parameter" of our model. In observations, the only way dark matter reveals its distribution is by the discrepancy between the observed rotation curves and the those predicted from the visible matter alone. We adopt the same approach; the dark matter is assumed to have a distribution which reproduces $V(r)$ given $\rho_*(r,z)$ and $\rho_g(r,z)$.
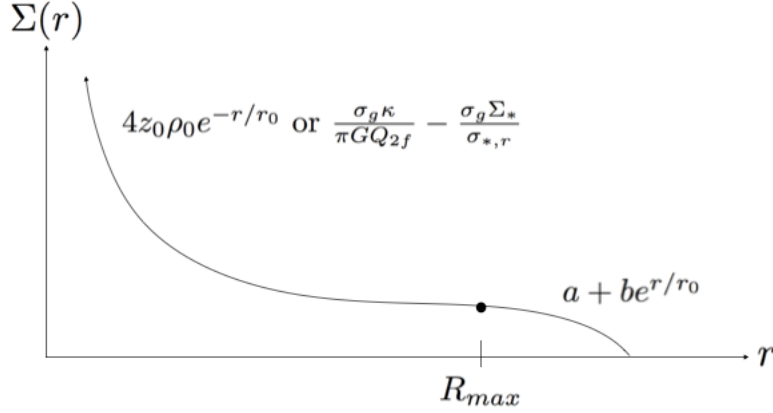
Figure 2: A visualisation of equation (52) which extends the stellar and mass distributions beyond R_{max} to ensure a smooth truncation to the disk

2.2 Limitations

Alas, the truth is never pure and rarely simple. I claimed the constant Q model had "encouraging," not "overwhelming" success in the introduction. Indeed, to make our model more realistic, it must be adjusted in multiple ways, mostly in the inner and outer parts of galaxies. These adjustments are paramount for finding g_{bar} because it's an integrated quantity; it relies on the model being accurate everywhere. Some past work (e.g. Meurer, Zheng & de Blok, 2013; Zheng et al., 2013) could ignore the constant Q model's deficiencies because they focused only on local quantities; we have no such luxury.

Often, to maintain constant Q, a galaxy requires starburst level gas densities in its centre, where as most do not have long term starbursts (Wong et al., 2016). Indeed, while Q remains roughly constant for large swathes of galaxies, it rises, sometimes quite significantly, in the very inner and outer parts (Meurer, Zheng & de Blok, 2013; Zheng et al., 2013). Therefore, to prevent our models from predicting unrealistically high gas densities at their centres, we decided for $r < r_0$, $\Sigma_g(r)$ will be a linear tangent extrapolation to the $\Sigma_g(r)$ profile at $r = r_0$.

Moving to the outer parts, matter cannot simply disappear at R_{max}. Its distribution is truncated for $r > R_{max}$, but $\rho_*(r, z)$ and $\rho_g(r, z)$ must still fall to 0 in a smooth manner (our inner pure mathematician interjects at this point to clarify that "smooth" is intended in the "English language" sense of the word and not the mathematical meaning of infinite differentiability). We redefined the stellar and gas surface mass densities as

$$\Sigma_*(r) = \begin{cases} 4z_0\rho_0 e^{-r/r_0} & 0 \leq r \leq R_{max} \\ \max(a_* + b_* e^{r/r_0},\, 0) & r \geq R_{max} \end{cases} \tag{51}$$

$$\Sigma_g(r) = \begin{cases} \frac{\sigma_g \kappa}{\pi G Q_{2f}} - \frac{\sigma_g \Sigma_*}{\sigma_{*,r}} & 0 \leq r \leq R_{max} \\ \max(a_g + b_g e^{r/r_0},\, 0) & r \geq R_{max} \end{cases} \tag{52}$$

with a_*, b_*, a_g and b_g fit such that Σ_* and Σ_g are continuously differentiable for $r < R_f$ with R_f defined as the radius such that $\Sigma_*(r) = \Sigma_g(r) = 0$ for all $r \geq R_f$, i.e. the disk ends at R_f even after the $a + be^{r/r_0}$ extensions are added. Figure 2 visualises the rather convoluted definition I just gave. Note, defining R_f implicitly assumes $\Sigma_*(r)$ and $\Sigma_g(r)$ are decreasing at $r = R_{max}$. Without these extensions to the Σ_* and Σ_g profiles, the gravitational force would have a sudden and unrealistic rise for $r \approx R_{max}$. Intuitively, this is because particles at R_{max} would not be experiencing any outward force at all where as particles closer to the centre experience forces inwards and outwards due to other particles on either side. One often assumes particles only feel the force of other particles at lower radii, but this is only true if the mass distribution has spherical symmetry; it is folly for the cylindrical symmetry of galaxies.

Finally, our models are built upon a single independent variable. It is curious such models were possible since dark matter halos are thought to be set by two parameters - V_{max} and "concentration," c, which are proxies for mass and angular momentum respectively. Perhaps the discrepancy is an indication of oversimplification somewhere in our models.
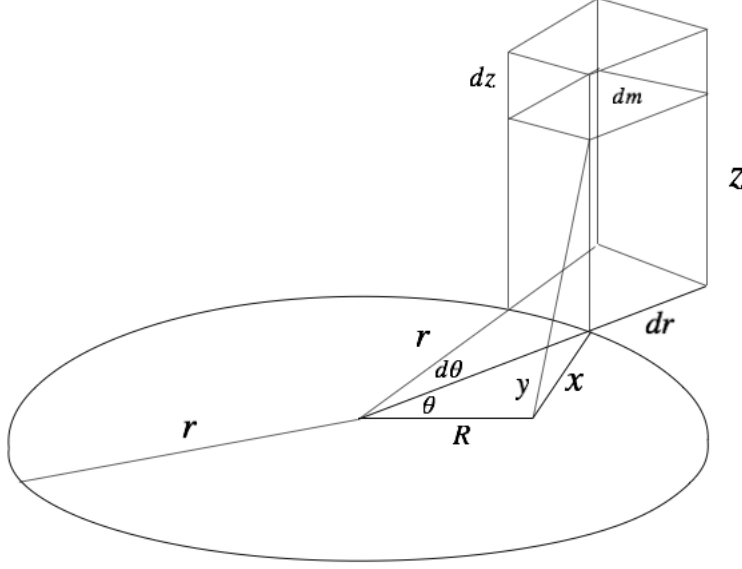
Figure 3: A visual aid for setting up equation (57) regarding $d\Phi_{bar}$

2.3 Deducing physical quantities

In testing MDAR, the two paramount quantities are the radial acceleration observed and that due to the baryons alone, g_{obs} and g_{bar} respectively. Throughout both MLS16 and our paper, it is assumed we are only dealing with rotationally supported galaxies and hence disk objects are travelling in perfect circles around the galactic centre, barring any local perturbations. Therefore,

$$g_{obs} = \frac{V(r)^2}{r} \tag{53}$$

at each radius, r, with $V(r)$ deduced from the URC, equation (4). The simplest way to find g_{bar} is via the gravitational potential of the baryons, Φ_{bar}. Then,

$$g_{bar} = -\frac{\partial \Phi_{bar}}{\partial R} \tag{54}$$

From figure 3, for a 3D, volume mass distribution, $\rho(r, z)$, the gravitational potential a distance R along the galaxy's midplane is

$$d\Phi = -\frac{G\,dm}{y} \tag{55}$$

$$= -\frac{G\rho r\,dz d\theta dr}{\sqrt{z^2 + x^2}} \tag{56}$$

$$= -\frac{G\rho r\,dz d\theta dr}{\sqrt{z^2 + r^2 + R^2 - 2rR\cos\theta}} \tag{57}$$

If $\rho(r, z) = \rho_{bar}(r, z) = \rho_*(r, z) + \rho_g(r, z)$ is the volume mass density of the baryons.

$$\Phi_{bar} = \int_0^\infty \int_0^{2\pi} \int_{-\infty}^\infty -\frac{G\rho r\,dz d\theta dr}{\sqrt{z^2 + r^2 + R^2 - 2rR\cos\theta}} \tag{58}$$

$$= -4\int_0^{R_f} \int_0^\pi \int_0^\infty \frac{G\rho r\,dz d\theta dr}{\sqrt{z^2 + r^2 + R^2 - 2rR\cos\theta}} \tag{59}$$

8

$$\therefore g_{bar} = -\frac{\partial \Phi_{bar}}{\partial R} \tag{60}$$

$$= 4\frac{\partial}{\partial R} \int_0^{R_f} \int_0^\pi \int_0^\infty \frac{G\rho r\, dz d\theta dr}{\sqrt{z^2 + r^2 + R^2 - 2rR\cos\theta}} \tag{61}$$

$$= 4 \int_0^{R_f} \int_0^\pi \int_0^\infty \frac{\partial}{\partial R} \frac{G\rho r\, dz d\theta dr}{\sqrt{z^2 + r^2 + R^2 - 2rR\cos\theta}} \tag{62}$$

$$= -4 \int_0^{R_f} \int_0^\pi \int_0^\infty \frac{G\rho r(R - r\cos\theta)\, dz d\theta dr}{(z^2 + r^2 + R^2 - 2rR\cos\theta)^{3/2}} \tag{63}$$

$$= -4G \int_0^{R_f} r \int_0^\pi (R - r\cos\theta) \int_0^\infty \frac{\rho\, dz d\theta dr}{(z^2 + r^2 + R^2 - 2rR\cos\theta)^{3/2}} \tag{64}$$

We have few options but to evaluate this integral numerically for the deduced mass distribution of baryons, $\rho_{bar}(r, z)$. Unfortunately, we are forced to cut-off the dz integral because computers can't deal with ∞; we've chosen to do so at 6 scale heights because $\mathrm{sech}^2(z/2z_0)|_{z=6z_0} = 0.01$.

To check for consistency with various cosmological models or observations (see section 3) one may wish to deduce the implied dark matter density at each radius. It can be done by Poisson's equation, $\nabla^2\Phi = 4\pi G\rho$. Using the Laplacian in spherical polar coordinates for a spherically symmetric function,

$$4\pi G\rho(r) = \frac{1}{r^2}\frac{d}{dr}\left(r^2\frac{d\Phi}{dr}\right) \tag{65}$$

$$\therefore \rho(r)_{DM} = \frac{1}{2\pi Gr}\frac{d\Phi_{DM}}{dr} + \frac{1}{4\pi G}\frac{d^2\Phi_{DM}}{dr^2} \tag{66}$$

We can deduce $\frac{d\Phi_{DM}}{dr}$, and hence $\frac{d^2\Phi_{DM}}{dr^2}$ by

$$\frac{d\Phi_{DM}}{dr} = g_{DM} \tag{67}$$

$$= g_{obs} - g_{bar} \tag{68}$$

both of which are know from equations (53) and (64) respectively. I reprise this method of recovering ρ_{DM} again in section 6 for a more complete exploration of its implications.

3 Example galaxy models

I'd like to present some example galaxies built via the prescription in section 2. I present a low, moderate and high mass galaxy corresponding to $V_{final} = 75\,km/s, 165\,km/s$ and $255\,km/s$ respectively. In figures 6, 10 and 14, I've removed the dark matter density data for the first scale length because the dark matter profile is cuspy; if I had plotted the complete data, the graph would look similar to step function due to the axis ranges. With the first scale length removed, all three are well fit by a cored isothermal sphere profile as shown. Another trend visible across the examples - figures 4, 8, 12, 5, 9 and 13 - is the increasing amount and influence of gas as V_{final} reduces.

Figures 7, 11 and 15 show how different galaxies trace out different regions of the $g_{bar} - g_{obs}$ plane. Exactly like MLS16, by putting together data from multiple different galaxies, we can fill a large extent of the relation. However, these figures show eccentric twists to the $g_{bar} - g_{obs}$ curve of each galaxy in its inner parts. I believe the problem is a combination of rotation curves being somewhat uncertain and constant Q being somewhat shaky - even after my adjustment - in galaxies' centres. Following Meurer, Zheng & de Blok (2013), it might be best considering only the middle 50% of a galaxy's radial range in the MDAR plots.

Overall, I don't think there are any great surprises found in our example galaxies.
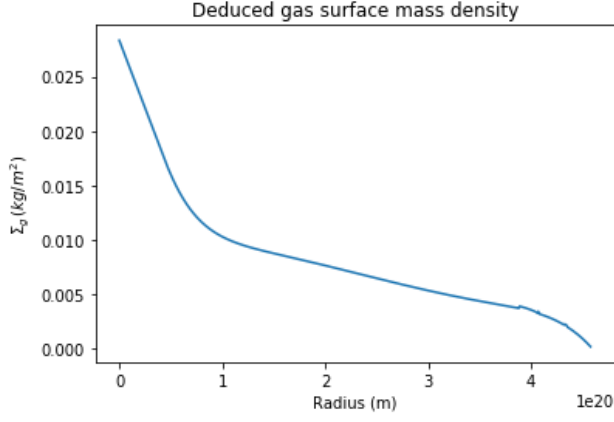
Figure 4: The gas surface mass density profile for a galaxy with $V_{final} = 75\,km/s$ as per equation (29)

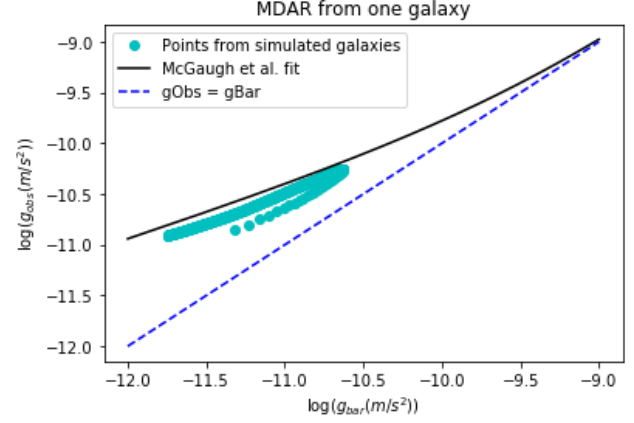Figure 7: g_{obs} versus g_{bar} in a galaxy with $V_{final} = 75\,km/s$ compared to the best fit curve to MLS16's data

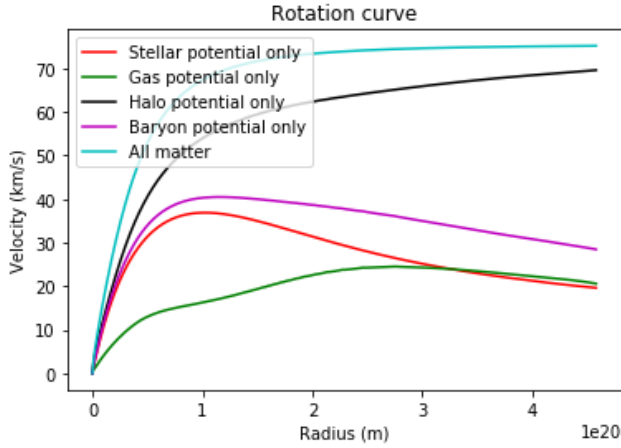
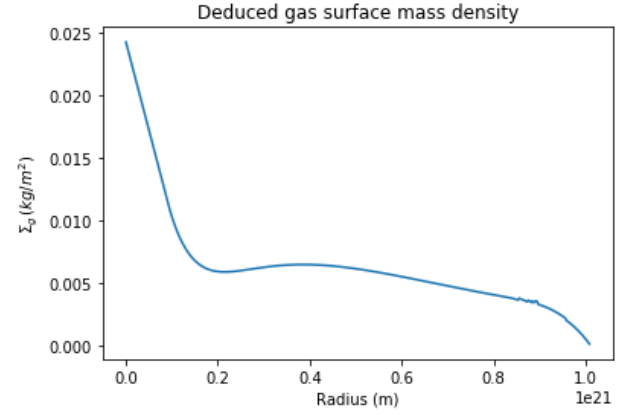Figure 5: The rotation curves due to each component for a galaxy with $V_{final} = 75\,km/s$

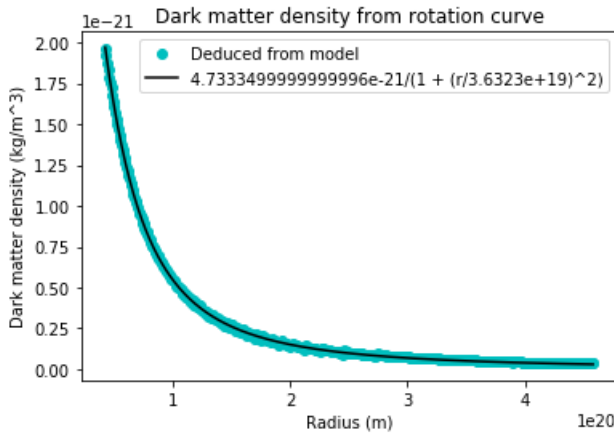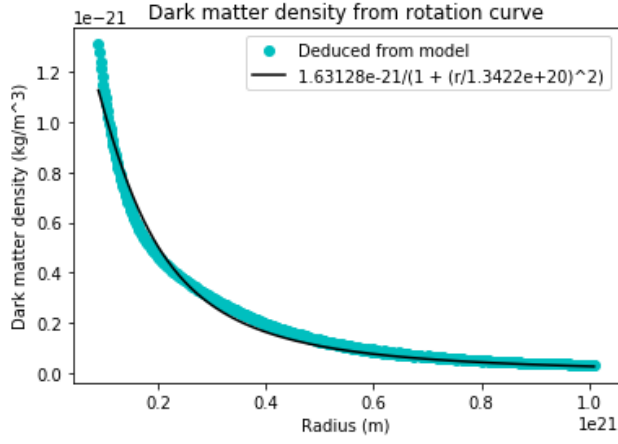Figure 8: The gas surface mass density profile for a galaxy with $V_{final} = 165\,km/s$ as per equation (29)

Figure 6: The implied dark matter density for a galaxy with $V_{final} = 75\,km/s$ as per equation (66)
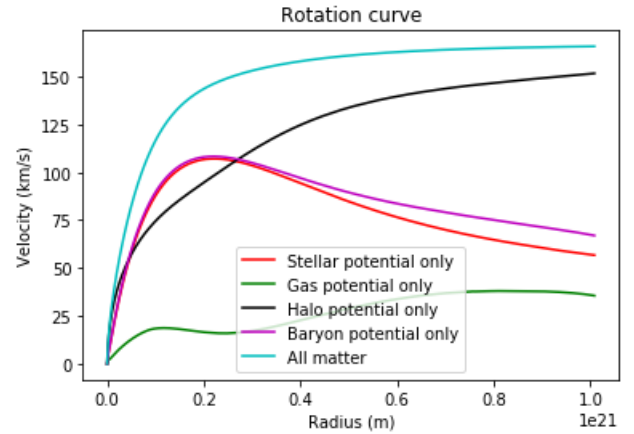
Figure 9: The rotation curves due to each component for a galaxy with $V_{final} = 165\,km/s$

10

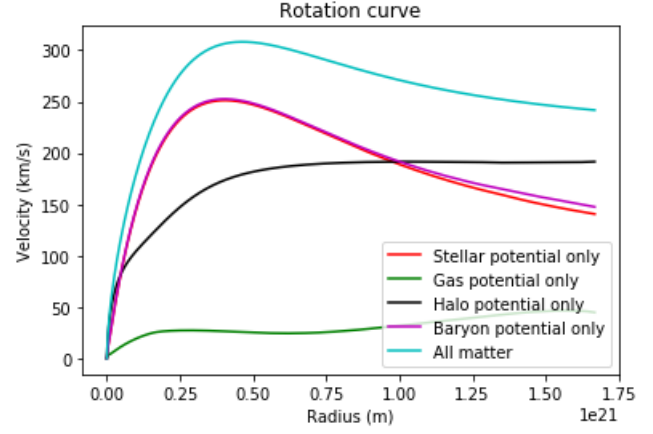Figure 10: The implied dark matter density for a galaxy with $V_{final} = 165\,km/s$ as per equation (66)

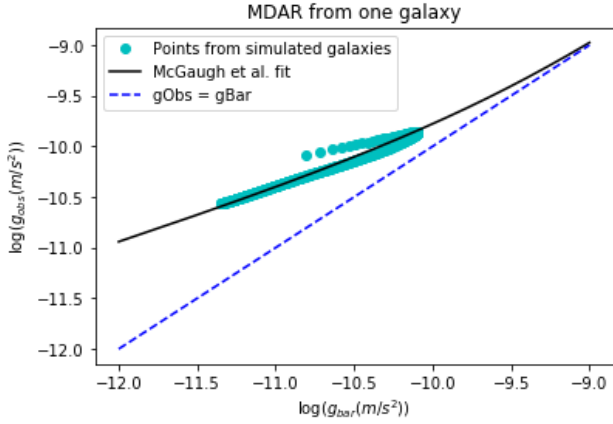Figure 13: The rotation curves due to each component for a galaxy with $V_{final} = 255\,km/s$

Figure 11: g_{obs} versus g_{bar} in a galaxy with $V_{final} = 165\,km/s$ compared to the best fit curve to MLS16's data
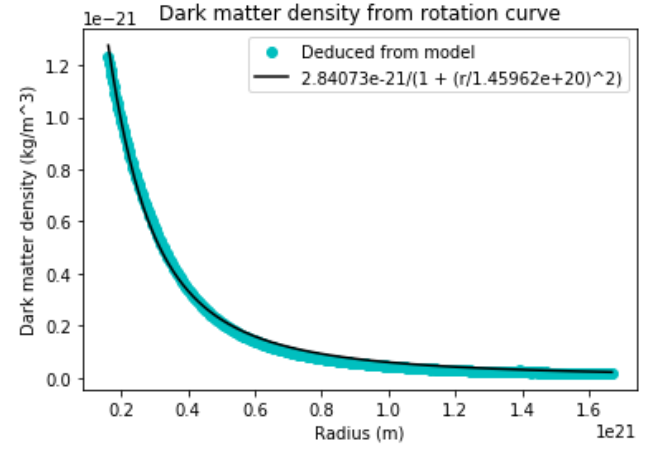

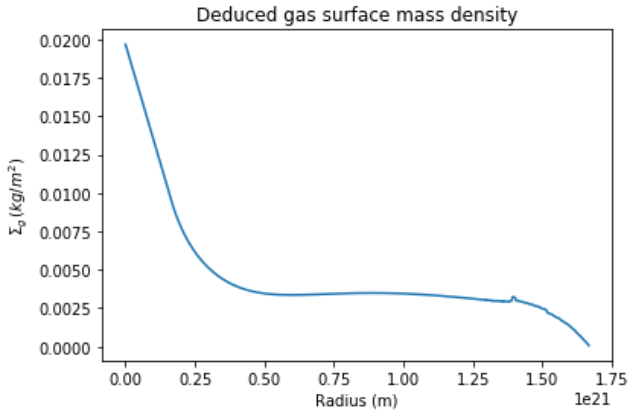Figure 14: The implied dark matter density for a galaxy with $V_{final} = 255\,km/s$ as per equation (66)

Figure 12: The gas surface mass density profile for a galaxy with $V_{final} = 255\,km/s$ as per equation (29)

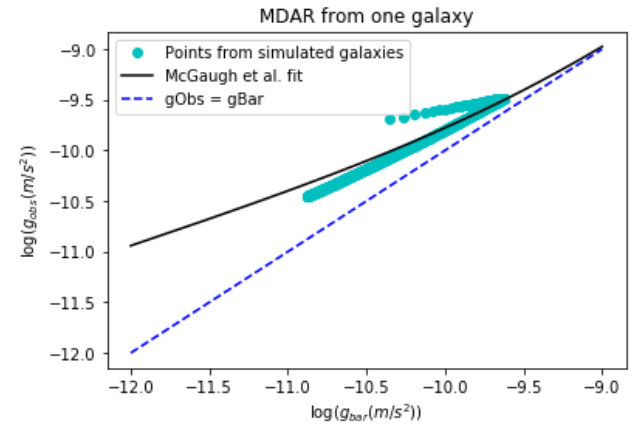

Figure 15: g_{obs} versus g_{bar} in a galaxy with $V_{final} = 255\,km/s$ compared to the best fit curve to MLS16's data
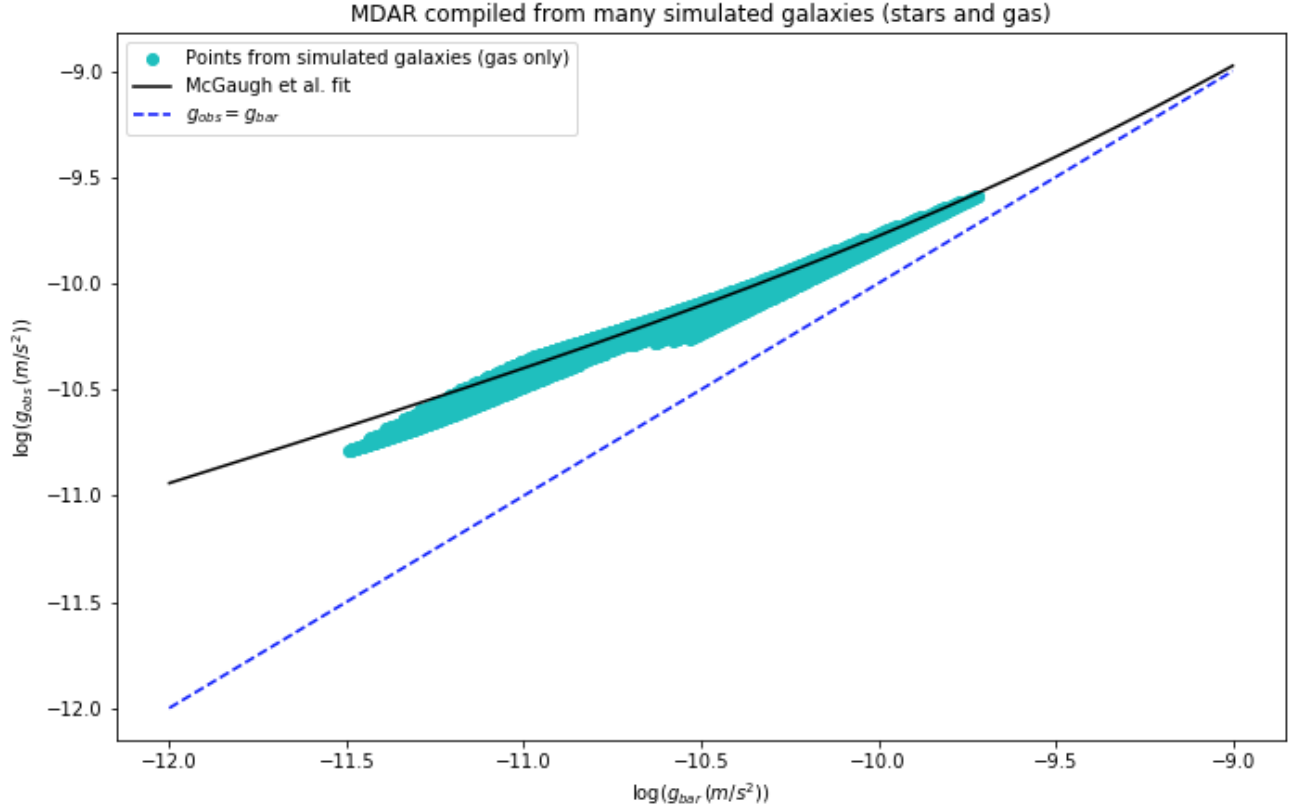
Figure 16: The MDAR compiled from our model galaxies using the prescription in section 2. The cyan is actually composed of individual data points from our model but they are so close together it looks like a continuous region.

4 Effect of constant Q on MDAR

Finally, I was ready to compile the MDAR curves traced by model galaxies with the full range of V_{final} allowed by the URC. On face value, the result (figure 16) looks excellent. However, figure 16 must be taken with a pinch of salt. I've only plotted the middle 50% of each model galaxy's radial range as suggested earlier; with the complete data, the result is less clear. Yet, limitations on radial range were the least of our concerns. About seven weeks into my ten week studentship, we were informed our approach of reformulating MDAR in terms of existing observational results had already been attempted before. Most notably, Wheeler, Hopkins & Dore (2018) showed - albeit with slightly simplistic assumptions - MDAR was closely linked to the baryonic Tully Fisher relation (BTFR) - a variation of equation (15). The way we've used equation (15) couples the stars to the rotation curve, but says very little about the gas - the component we hypothesized to drive MDAR. Furthermore, it turns out Wheeler, Hopkins & Dore (2018) weren't even the first to connect MDAR with Tully Fisher - Yegorova & Salucci (2007) did it 12 years ago with their "radial Tully Fisher relation." To get over our denial, we remade figure 16 but with stars only (figure 17) and then with gas only (figure 18) to isolate the effects of the two.   Figure 17 shows exemplary agreement between the MDAR traced by stars and MLS16's result. Furthermore, almost the full radial extent is usable because the stable disk model's limitations only affect gas. The antithesis of figure 17's success is figure 18's failure. The $g_{bar} - g_{obs}$ relation traced by a galaxy with a single constant Q gas disk alone would not be mistaken for the curve of MLS16 by anyone. Figure 18 shows g_{bar} due to a constant Q disk hardly responds to the g_{obs} set by the rotation curve.

The writing was on the wall. Constant Q is not the physical basis underlying MDAR as hypothesised. Instead, it's a distraction from the more fundamental relation between Tully Fisher and MDAR.
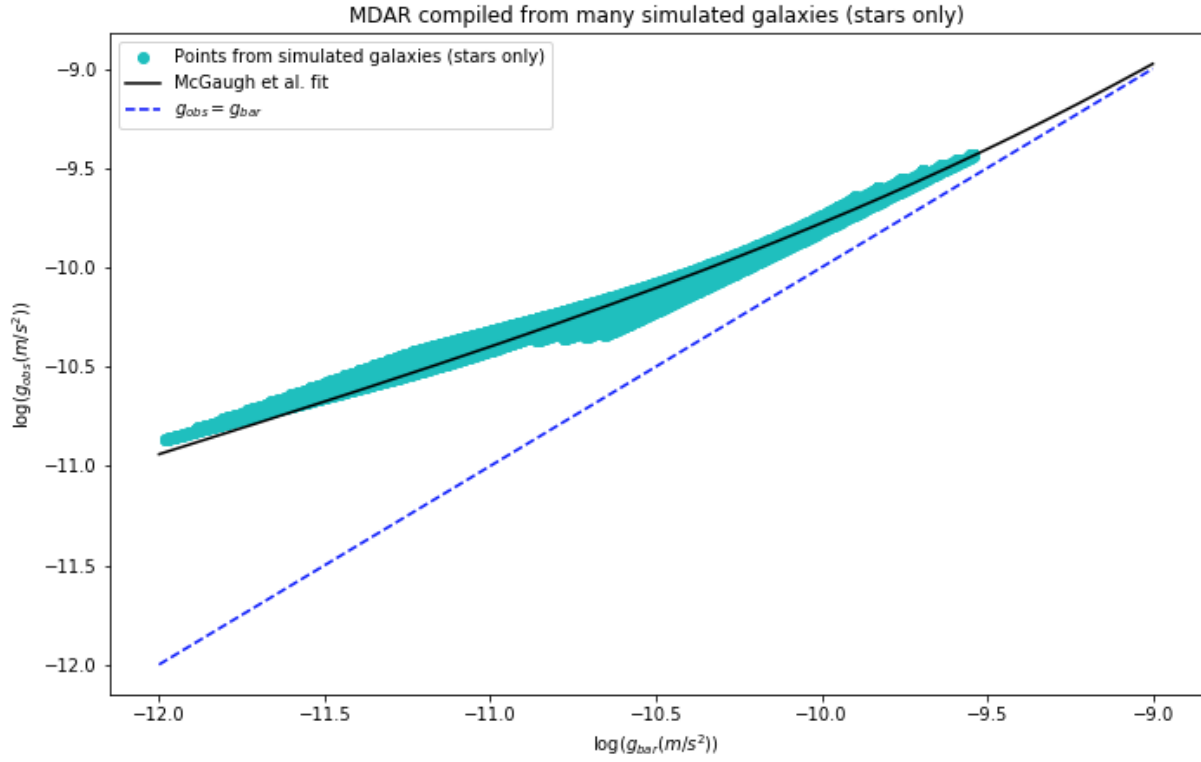
Figure 17: MDAR compiled from our model galaxies but with stars only ($g_{bar} = g_*$) to isolate the relationship between the stellar disk and MDAR
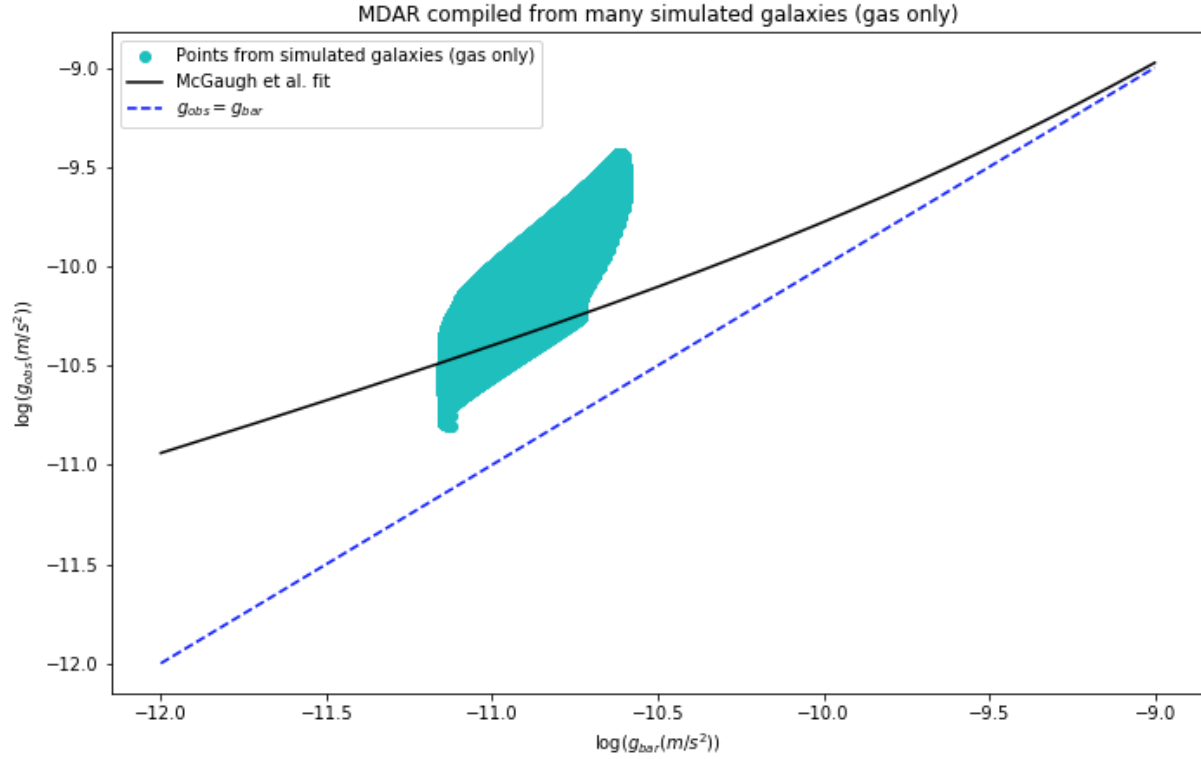

Figure 18: MDAR compiled model galaxies containing a constant stability gas disk alone ($g_{bar} = g_{gas}$) to see whether constant Q is really driving MDAR
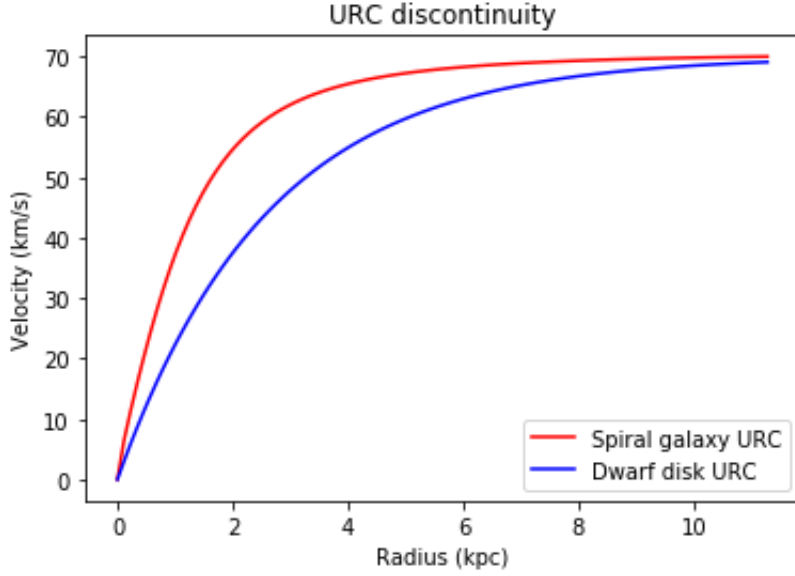
Figure 19: The differing rotation curves generated by the URC of spiral and dwarf disk galaxies

.

5 A note on the "universal" rotation curve

I cannot conclude discussions on the stable disk model without noting a caveat to the URC. Assumptions about the rotation curve fundamentally affect $\rho_g(r, z)$ because the epicycle frequency,

$$\kappa(r) = \frac{V(r)}{r}\sqrt{2\left(1 + \frac{r}{V(r)}\frac{dV(r)}{dr}\right)} \tag{69}$$

relies heavily upon $V(r)$. We found it worth reflecting on the assumed rotation curve. The URC as quoted in equation (4) is only calibrated for spiral galaxies and there have been multiple attempts to extend the URC to accommodate for dwarf disk galaxies (Karukes & Salucci, 2016; Salucci et al., 2012; Kapferer et al., 2006) with the most recent and successful being Karukes & Salucci (2016). Frankly, their paper was very difficult to understand. Rather than invoking their mysterious "compactness" parameter which hardly changes between galaxies and has only a very small impact on the predicted rotation curves, I fit my own curve to their normalised data and de-normalised it by simply scaling by V_{max} and R_{opt} as predicted by our models. My fit to their data was

$$V(r) = V_{max}(1 - e^{-r/1.9905r_0}) \tag{70}$$

I felt there may be some physical significance that $1.9905 \approx 2$ and the "true curve" may be $V(r) = V_{max}(1 - e^{-r/2r_0})$. Sadly, the dwarf disk extension to the URC, equation (70), does not continuously match on to the URC of spiral galaxies, equation (4). The boundary between the two regimes is $V_{max} \approx 70\,km/s$. As figure (19) shows, the two regimes give somewhat different rotation curves. Therefore, the URC is not as "universal" as it's made out to be. Furthermore, it may indicate oversimplification in the URC. As previously mentioned in section 2.2, dark matter halos are said to be built from two parameters where as the URC and our models are built from only one. The variation in slope between the two URCs in figure 19 suggests another independent variable is required to encompass the true variety of rotation curves.

6 Final remarks on MDAR

By the end of the project, I felt the literature regularly framed the relationship between MDAR and dark matter distribution as indirect. Yet, it may not be. MLS16's results are popularised in the form

$$g_{obs} = \frac{g_{bar}}{1 - e^{-\sqrt{g_{bar}/g_\dagger}}} \tag{71}$$

However, MDAR can be rephrased as a link between the acceleration due to baryonic matter and the acceleration due to the implied dark matter.

$$g_{DM} = g_{obs} - g_{bar} \tag{72}$$

$$= \frac{g_{bar}}{1 - e^{-\sqrt{g_{bar}/g_\dagger}}} - g_{bar} \tag{73}$$

$$= \frac{g_{bar}}{e^{\sqrt{g_{bar}/g_\dagger}} - 1} \tag{74}$$

MLS16 only makes a passing reference to equation (74) and I feel its implications aren't fully appreciated. From g_{DM}, one can deduce the dark matter distribution, ρ_{DM}, via Poisson's equation. We may assume ρ_{DM}, and hence Φ_{DM}, are spherically symmetric. Whether we choose $g_{DM} = \frac{d\Phi_{DM}}{dr}$ or $g_{DM} = -\frac{d\Phi_{DM}}{dr}$ is only a sign convention and here I'm using the positive convention for all relevant relations to avoid confusing the issue. Therefore, applying the (now much simpler) form of the Laplacian in spherical polar coordinates,

$$4\pi G \rho_{DM} = \nabla^2 \Phi_{DM} \tag{75}$$

$$= \frac{1}{r^2} \frac{d}{dr} \left(r^2 \frac{d\Phi_{DM}}{dr} \right) \tag{76}$$

$$= \frac{2}{r} \frac{d\Phi_{DM}}{dr} + \frac{d^2 \Phi_{DM}}{dr^2} \tag{77}$$

$$= \frac{2g_{DM}}{r} + \frac{dg_{DM}}{dr} \tag{78}$$

$$= \frac{2g_{bar}}{r \left(e^{\sqrt{g_{bar}/g_\dagger}} - 1 \right)} + \frac{dg_{DM}}{dg_{bar}} \frac{dg_{bar}}{dr} \tag{79}$$

$$= \frac{2g_{bar}}{r \left(e^{\sqrt{g_{bar}/g_\dagger}} - 1 \right)} + \frac{e^{\sqrt{g_{bar}/g_\dagger}} - 1 - g_{bar} \left(\frac{1}{2\sqrt{g_{bar}g_\dagger}} e^{\sqrt{g_{bar}/g_\dagger}} \right)}{\left(e^{\sqrt{g_{bar}/g_\dagger}} - 1 \right)^2} \frac{dg_{bar}}{dr} \tag{80}$$

$$= \frac{2g_{bar}}{r \left(e^{\sqrt{g_{bar}/g_\dagger}} - 1 \right)} + \frac{e^{\sqrt{g_{bar}/g_\dagger}} \left(1 - \frac{1}{2} \sqrt{g_{bar}/g_\dagger} \right) - 1}{\left(e^{\sqrt{g_{bar}/g_\dagger}} - 1 \right)^2} \frac{dg_{bar}}{dr} \tag{81}$$

$$\therefore \rho_{DM} = \frac{g_{bar}}{2\pi G r \left(e^{\sqrt{g_{bar}/g_\dagger}} - 1 \right)} + \frac{e^{\sqrt{g_{bar}/g_\dagger}} \left(1 - \frac{1}{2} \sqrt{g_{bar}/g_\dagger} \right) - 1}{4\pi G \left(e^{\sqrt{g_{bar}/g_\dagger}} - 1 \right)^2} \frac{dg_{bar}}{dr} \tag{82}$$

These equations hold generally if we assume MDAR always holds. To get ρ_{DM} for actual galaxies, we must make measurements or observations of g_{bar}. As an algebraically simpler primer, I first consider the asymptotic behaviour of equation (82). If $g_{bar} \ll g_\dagger$, as it will be in the outer regions of all galaxies,

$$e^{\sqrt{g_{bar}/g_\dagger}} \approx 1 + \sqrt{g_{bar}/g_\dagger} \tag{83}$$

Furthermore,

$$g_{bar} \ll g_\dagger \implies \frac{g_{bar}}{g_\dagger} \ll 1 \implies \frac{g_{bar}}{g_\dagger} \ll \sqrt{\frac{g_{bar}}{g_\dagger}} \tag{84}$$

Therefore, for $g_{bar} \ll g_\dagger$,

$$\rho_{DM} \approx \frac{g_{bar}}{2\pi G r \sqrt{g_{bar}/g_\dagger}} + \frac{(1 + \sqrt{g_{bar}/g_\dagger})(1 - \frac{1}{2}\sqrt{g_{bar}/g_\dagger}) - 1}{4\pi G g_{bar}/g_\dagger} \frac{dg_{bar}}{dr} \tag{85}$$

$$= \frac{g_{bar}}{2\pi G r \sqrt{g_{bar}/g_\dagger}} + \frac{1 - \frac{1}{2}\sqrt{g_{bar}/g_\dagger} + \sqrt{g_{bar}/g_\dagger} - \frac{1}{2}g_{bar}/g_\dagger - 1}{4\pi G g_{bar}/g_\dagger} \frac{dg_{bar}}{dr} \tag{86}$$

$$= \frac{g_{bar}}{2\pi G r \sqrt{g_{bar}/g_\dagger}} + \frac{\sqrt{g_{bar}/g_\dagger} - g_{bar}/g_\dagger}{8\pi G g_{bar}/g_\dagger} \frac{dg_{bar}}{dr} \tag{87}$$

$$\approx \frac{g_{bar}}{2\pi G r \sqrt{g_{bar}/g_\dagger}} + \frac{\sqrt{g_{bar}/g_\dagger}}{8\pi G g_{bar}/g_\dagger} \frac{dg_{bar}}{dr} \tag{88}$$

$$= \frac{\sqrt{g_{bar}g_\dagger}}{2\pi G r} + \frac{1}{8\pi G} \sqrt{\frac{g_\dagger}{g_{bar}}} \frac{dg_{bar}}{dr} \tag{89}$$

Generally, in the outskirts of galaxies, the rotation curve due to baryons alone is very close to Keplerian. Hence, we can approximate g_{bar} as arising from a point mass, M, in regions where $g_{bar} \ll g_\dagger$. Then, one gets

$$g_{bar} = \frac{GM}{r^2} \tag{90}$$

$$\therefore \frac{dg_{bar}}{dr} = -\frac{2GM}{r^3} \tag{91}$$

Substituting these expressions into equation (89) yields

$$\rho_{DM} \approx \frac{\sqrt{\frac{GM}{r^2} g_\dagger}}{2\pi Gr} - \frac{1}{8\pi G} \sqrt{\frac{g_\dagger r^2}{GM}} \frac{2GM}{r^3} \tag{92}$$

$$= \frac{1}{2\pi r^2} \sqrt{\frac{Mg_\dagger}{G}} - \frac{1}{4\pi r^2} \sqrt{\frac{Mg_\dagger}{G}} \tag{93}$$

$$= \frac{1}{4\pi r^2} \sqrt{\frac{Mg_\dagger}{G}} \tag{94}$$

Therefore, if MDAR holds indefinitely in a galaxy, the dark matter distribution must converge on the $\rho_{DM} \propto \frac{1}{r^2}$ of an isothermal sphere, but not the $\rho_{DM} \propto \frac{1}{r^3}$ typical of dark matter simulations. Equivalently, if MDAR holds indefinitely, then rotation curves must remain flat indefinitely, unlike the eventually declining rotation curves predicted by dark matter simulations.

Having examined the asymptotic behaviour, I shifted my focues to the complete radial range. We can approximate g_{bar} as arising from a thin, pure exponential disk - whose surface mass density is given by $\Sigma(r) = \Sigma_0 e^{-r/r_0}$. This assumption forces one to ignore low mass galaxies because gas would have a non-negligible contribution to g_{bar}. I accept this constraint because the gas distribution in galaxies is disputed anyway (e.g. notice the contrast between our stable disk approach and the approach taken by Karukes & Salucci, 2016, in their mass modelling). Therefore, assumptions made about gas may compromise our subsequent deductions. By focusing on medium to high mass galaxies, the gas contribution can be more or less ignored. Serendipitously, a thin exponential disk allows analytic subsequent analysis. Finally, defining $x = \frac{r}{2r_0}$ and letting I and K be the modified Bessel functions of the first and second kind respectively, Freeman (1970) derives equation (95).

$$g_{bar} = \frac{\pi G \Sigma_0 r}{r_0} \left(I_0(x) K_0(x) - I_1(x) K_1(x) \right) \tag{95}$$

$$\therefore \frac{dg_{bar}}{dr} = \frac{g_{bar}}{r} + \frac{\pi G \Sigma_0 r}{2r_0^2} \left(I_1(x) K_0(x) - I_0(x) K_1(x) - \frac{1}{2} K_1(x) \Big(I_0(x) + I_2(x) \Big) + \frac{1}{2} I_1(x) \Big(K_0(x) + K_2(x) \Big) \right) \tag{96}$$

Substituting equations (95) and (96) into equation (82) yields the implied dark matter distribution for an exponential disk galaxy which strictly follows MDAR. Past the first several scale lengths, the result must converge on equation (94) with $M = 2\pi\Sigma_0 r_0^2$ for an exponential disk. However, ρ_{DM} from equation (82) is not particularly insightful on its own. Much of the fuss regarding dark matter density profiles is about the exponent of their best power law fit, r^α, in different regions. The most important topics are the power law exponent in the very inner and outer parts of galaxies. To find α, I found $\frac{d\ln\rho_{DM}}{d\ln r}$ - a task so tedious it might be too cruel as a torture technique for misbehaving calculus students. Using equation (82),

$$\frac{d\ln\rho_{DM}}{d\ln r} = \frac{d\ln\rho_{DM}}{d\rho_{DM}}\frac{d\rho_{DM}}{dr}\frac{dr}{d\ln r} \tag{97}$$

$$= \frac{r}{\rho_{DM}}\frac{d\rho_{DM}}{dr} \tag{98}$$

$$= \frac{r}{\rho_{DM}}\frac{d}{dr}\left(\frac{g_{bar}}{2\pi Gr\left(e^{\sqrt{g_{bar}/g_\dagger}}-1\right)} + \frac{e^{\sqrt{g_{bar}/g_\dagger}}\left(1-\frac{1}{2}\sqrt{g_{bar}/g_\dagger}\right)-1}{4\pi G\left(e^{\sqrt{g_{bar}/g_\dagger}}-1\right)^2}\frac{dg_{bar}}{dr}\right) \tag{99}$$

$$= \frac{r}{\rho_{DM}}\left[-\frac{g_{bar}}{2\pi r^2\left(e^{\sqrt{g_{bar}/g_\dagger}}-1\right)} + \frac{e^{\sqrt{g_{bar}/g_\dagger}}\left(1-\frac{1}{2}\sqrt{g_{bar}/g_\dagger}\right)-1}{2\pi Gr\left(e^{\sqrt{g_{bar}/g_\dagger}}-1\right)^2}\frac{dg_{bar}}{dr}+\right. \tag{100}$$

$$\frac{1}{4\pi G\left(e^{\sqrt{g_{bar}/g_\dagger}}-1\right)^4}\left\{\left(e^{\sqrt{g_{bar}/g_\dagger}}-1\right)^2\left(\frac{1}{2\sqrt{g_{bar}g_\dagger}}e^{\sqrt{g_{bar}/g_\dagger}}(1-\frac{1}{2}\sqrt{g_{bar}/g_\dagger})-\frac{1}{4}e^{\sqrt{g_{bar}/g_\dagger}}\sqrt{\frac{1}{g_{bar}g_\dagger}}\right)\right. \tag{101}$$

$$\left.-2(e^{\sqrt{g_{bar}/g_\dagger}}-1)\left(\frac{1}{2}\sqrt{g_{bar}/g_\dagger}e^{\sqrt{g_{bar}/g_\dagger}}\right)\left(e^{\sqrt{g_{bar}/g_\dagger}}(1-\frac{1}{2}\sqrt{g_{bar}/g_\dagger})-1\right)\right\}\left(\frac{dg_{bar}}{dr}\right)^2 \tag{102}$$

$$\left.+\frac{e^{\sqrt{g_{bar}/g_\dagger}}(1-\frac{1}{2}\sqrt{g_{bar}/g_\dagger})-1}{4\pi G(e^{\sqrt{g_{bar}/g_\dagger}}-1)^2}\frac{d^2g_{bar}}{dr^2}\right] \tag{103}$$

which requires equations (95) and (96) to get

$$\frac{d^2g_{bar}}{dr^2} = -\frac{g_{bar}}{r^2} + \frac{1}{r}\frac{dg_{bar}}{dr} + \frac{\pi G\Sigma_0}{2r_0^2}\left(I_1(x)K_0(x)-I_0(x)K_1(x)-\frac{1}{2}K_1(x)\Big(I_0(x)+I_2(x)\Big)+\frac{1}{2}I_1(x)\Big(K_0(x)+K_2(x)\Big)\right) \tag{104}$$

$$+\frac{\pi G\Sigma_0 r}{4r_0^3}\left[\frac{1}{2}\Big(I_0(x)+I_2(x)\Big)K_0(x)-2I_1(x)K_1(x)+\frac{1}{2}\Big(K_0(x)+K_2(x)\Big)I_0(x)\right. \tag{105}$$

$$+\frac{1}{2}\Big(K_0(x)+K_2(x)\Big)\Big(I_0(x)+I_2(x)\Big)-\frac{1}{2}K_1(x)\Big(I_1(x)+\frac{1}{2}(I_1(x)+I_3(x))\Big) \tag{106}$$

$$\left.-\frac{1}{2}I_1(x)\Big(K_1(x)+\frac{1}{2}(K_1(x)+K_3(x))\Big)\right] \tag{107}$$

I doubt anybody understands anything by looking at equations (103) and (107). I've included them solely for rigour and so that no other poor soul has to spend an eternity deriving the equations to reproduce, or build upon, figure (20) which visualises $d\ln\rho_{DM}/d\ln r$. Using the scaling relations from previous sections, a galaxy with $75\,km/s \leq V_{final} \leq 255\,km/s$ has M_* and r_0 between $2.5\times10^{39}kg - 4.7\times10^{41}kg$ and $4.3\times10^{19} - 1.6*10^{20}m$ respectively. To account for scaling relations' scatter and the effect of disk thickness - which reduces g_{bar}'s amplitude but has little effect on its shape - I've plotted $d\ln\rho_{DM}/dr\ln r$ (figure 20) for galaxies with a varied combination of M_* and r_0 - including galaxies with unrealistically low and high r_0 for their stellar mass. $d\ln\rho_{DM}/d\ln r$ is not monotone decreasing in any case as it should be in popular dark matter profile such as NFW, Burkert, cored isothermal sphere or "DC13" (Di Cintio et al., 2013). For the galaxies with the lowest r_0, the power law exponent, $d\ln\rho_{DM}/d\ln r$, rises briefly and then falls to -2. For the remaining 20 galaxies, $d\ln\rho_{DM}/d\ln r$ has more or less the same shape - a steady decline from about -0.75 to -2.25 back up to -2; it is a distinctive shape completely different from the aforementioned dark matter profiles.

The results of figure 20 are significant because MDAR is a universal MOND law. If MOND is correct, observations made under the assumption of ΛCDM must reproduce the dark matter density profiles implied by figure 20. Therefore, we may finally be able to settle the debate between MOND and dark matter because the two paradigms disagree on two salient features. First, rotation curves must stay indefinitely flat under MOND, as per equation (94), where as they must eventually decline under ΛCDM. Furthermore, the implied dark matter density profiles from ΛCDM have a monotonic decreasing $d\ln\rho_{DM}/d\ln r$ where as those implied by MOND have a characteristic dip to ≈ -2.25 and rise back to -2 for galaxies with moderate to large r_0. Both figure 20 and dark matter based simulations agree on one point - the inner dark matter profiles are cuspy, not cored as deduced in observations.

If I had more time, or thought of this idea earlier, I would have liked to explore the effect of the specific MOND
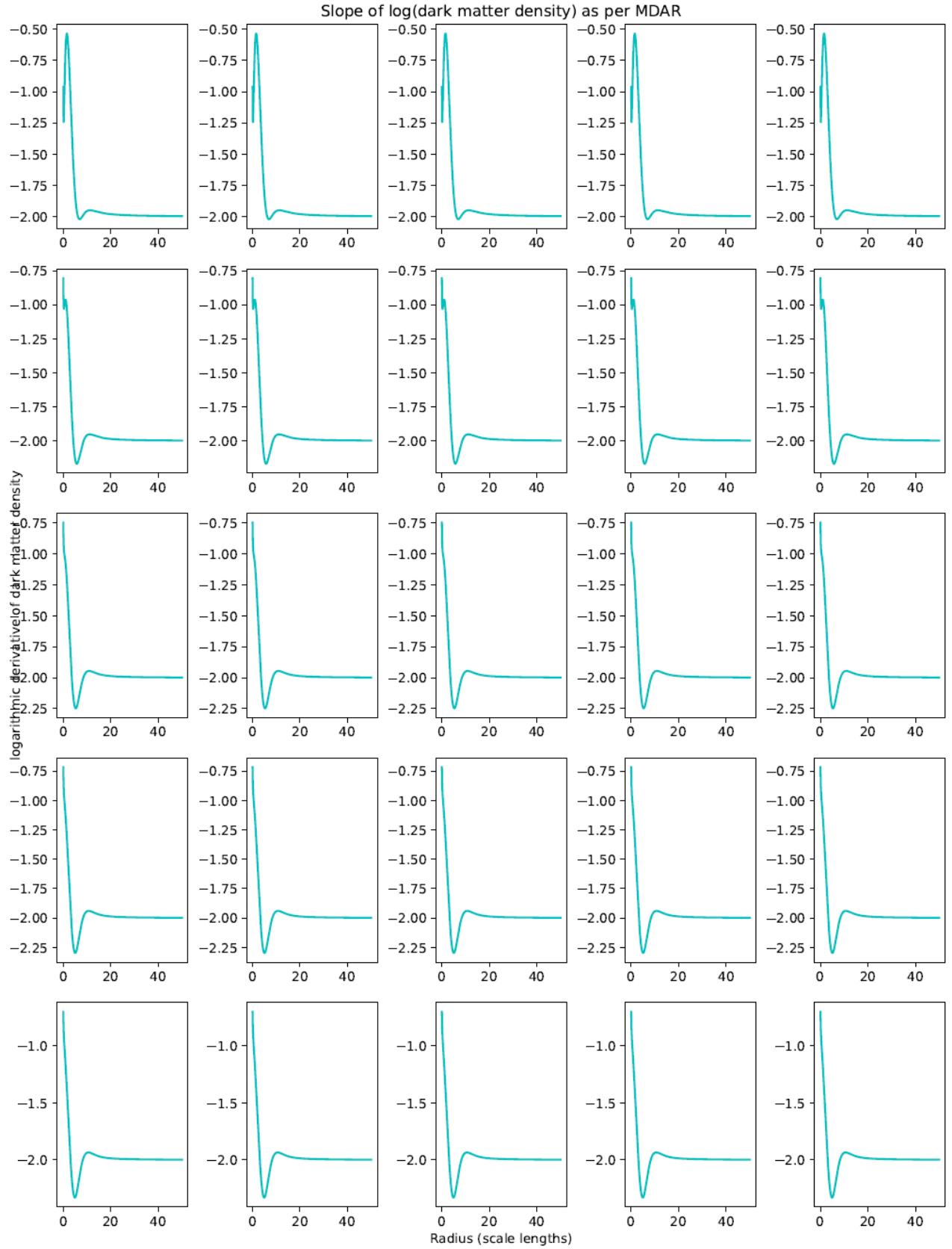
Figure 20: The graph at column i and row j (counting from the top left corner) contains $d \ln \rho_{DM} / d \ln r$ as per equations (103) and (107) for a galaxy with $M_* = (2.5 \times 10^{39} + (i-1) \times 10^{41}) \, kg$ and $r_0 = (4j-1) \times 10^{19} \, m$
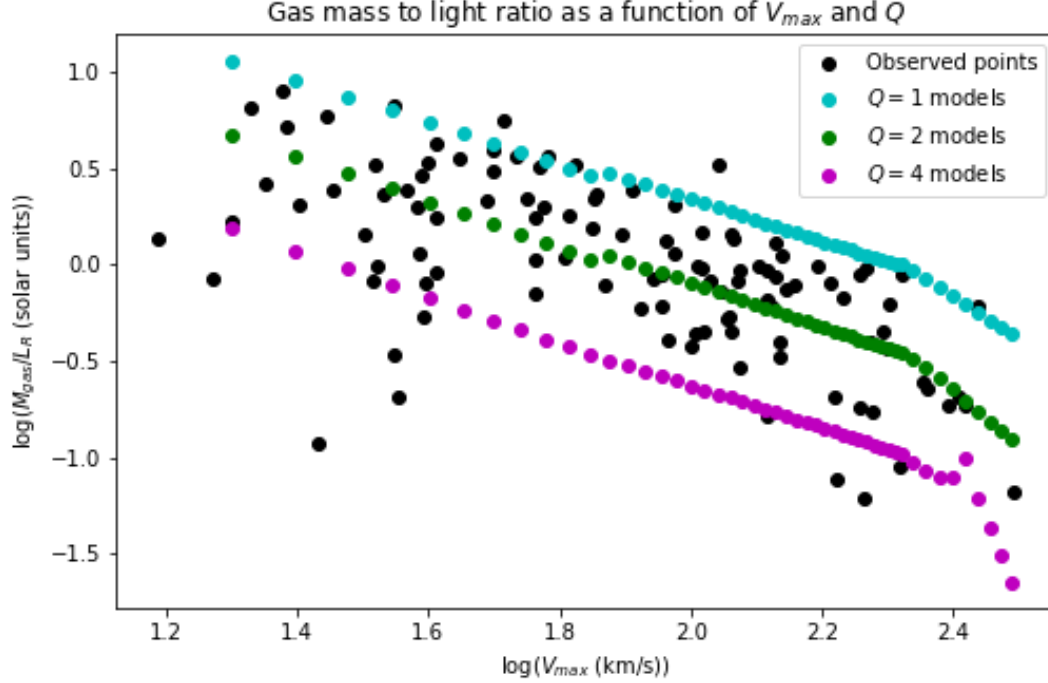
.

Figure 21: The gas mass to light ratio of HI selected galaxies forming SINGG. The constant Q model can account for the trend and scatter in the observed data by varying the value of Q_{2f} between the average and most extreme values observed in galaxies.

interpolating function on figure 20; Milgrom (2016a) shows several functional forms fit MLS16's data. I would also have liked to try Sersic profiles, rather than exponential disks, to find g_{bar} to account for a more holistic view of stellar disks. Similarly, I should try varying prescriptions for a 3D stellar disk just in case it has a significant impact on g_{bar}. Finally, we must acknowledge neither MOND nor ΛCDM may be correct. Warm dark matter, self-interacting dark matter, entropic gravity (which is really MOND), Debye gravitational theory etc. all provide compelling alternatives. The "correct" theory may be any of them, a combination of them or a new idea entirely.

7   Galaxy scaling relations

I still had a few weeks left on my internship by the time we came to be crestfallen with the negligible impact of stable disks on MDAR. We were left with well calibrated galaxy models, but little to do with them. The prevalence of scaling relations in astronomy is disconcerting to me. Most of them, including the ones we used, have next to no physical basis whatsoever. The classic case is the $\log - \log$ scatter plot with a best fit line whose slope defies all rational explanation. We agreed explaining galaxy scaling relations, even in terms of more fundamental relations as with MDAR, would be time well spent. The constant Q model may yet be the physical basis behind some of these other scaling relations, even though it wasn't responsible for MDAR.

We had at least one success to report. There is a correlation between the HI mass to light ratio and V_{max} for the HI selected galaxies forming SINGG. We converted the observed M_{HI}/L_R into M_{gas}/L_R by letting $M_{gas} = 1.3 M_{HI}$ and compared those values to M_{gas}/L_R from our model where L_R comes from equation (15) and M_{gas} is

$$M_{gas} = \int_0^{R_f} 2\pi r \Sigma_g(r) \, dr \qquad (108)$$

with Σ_g from equation (52) and the integral evaluated numerically. The spiral URC, equation (4), probes $V_{max} > 70 \, km/s$ and the dwarf disk URC, equation (70), probes $V_{max} < 70 \, km/s$ in our model. By letting $Q_{2f} = 2$, the average value of Q_{2f} observed in galaxies, our models fit the data very well as seen in figure 21. By varying Q_{2f} between 1 and 4, some of the most extreme values observed in galaxies, we were able to account for the scatter

in the relation. Therefore, it is very much possible constant Q_{2f} may be driving the trend and scatter in the $\log(M_{gas}/L_R) - \log(V_{max})$ relation. Alternatively, since $Q_{2f} = 2$ results in the best fit to the observed data, one can see it as justification for choosing $Q_{2f} = 2$ in our model. Rather than choose the average Q_{2f} observed, we could have calibrated our model to fit figure 21 instead.

Our results have a "kink" in them at $V_{max} \approx 210 \, km/s$ - the velocity at which the URC transitions from being strictly increasing to having a decreasing tail. I don't know if this kink is a physical insight from the constant Q model or an artefact of the URC. However, the idea of constant Q has revealed a possibility which would never be detected by simply fitting a line of best fit to a scatter plot.

8 Conclusion

My project finished far from where it began, but I enjoyed the journey nonetheless. It was disappointing our hypothesis about the constant Q model motivating MDAR failed, but it would have been naive to assume it would've worked a priori. Our failure simply reflects the far greater number of appealing theories than the number of correct ones. As Einstein put it, "if we knew what were doing, it wouldn't be called research." However, the models we build in section two are limited, but not incorrect. As we showed in section 7, the constant Q model still has its merits in explaining galaxy scaling relations and stimulating further study about their properties. Finally, I also made some remarks about the differences in implied dark matter profiles predicted by MOND and dark matter simulations. While my results have analytical rigour, I don't intuitively understand the eccentric shapes in figure 20. I'm still deciding whether I've made a mistake - be it algebraic, in my assumptions about a 2D disk, the chosen MOND interpolating function or something else entirely - or whether I have a result worthy of further exploration. Regarding the studentship as a whole, I've loved listening about all the different work within the astrophysics community (even if most discussions went way over my head) and I very much appreciate the guidance of Professor Meurer and thank him for choosing me for this project.

References

Di Cintio A., Brook C. B., Maccio A. V., Stinson G. S., Knebe A., Dutton A. A., Wadsley J., 2013, MNRAS, 437, 415

Freeman K. C., 1970, ApJ, 160, 811

Gentile G., Famaey B., de Blok W. J. G., 2011, A&A, 527, A76

Ianjamasimanana R., de Blok W. J. G., Walter F., Heald G. H., Caldu-Primo A., Jarrett T. H., 2015, AJ, 150, 47

Kapferer W., Kronberger T., Schindler S., Böhm A., Ziegler B. L., 2006, A&A, 446(3), 847

Kapteyn J. C. 1922, ApJ, 55, 302

Karukes E. V., Salucci P., 2016, MNRAS, 465, 4703

Keller, B. W., Wadsley J. W., 2016, arXiv preprint arXiv:1610.06183

Kennicutt R. C., 1989, ApJ 344, 685

Leroy A. K., Walter F., Brinks E., Bigiel F., De Blok W. J. G., Madore B., Thornley M. D., 2008, AJ, 136(6), 2782.

Ludlow et al., 2017, Physical Review Letters, 118(16), 161103

McGaugh S. S., Lelli F., Schombert J. M., 2016, Physical Review Letters, 117(20), 201101 (MLS16)

Meurer G. R., Zheng Z., de Blok W. J. G., 2013, MNRAS, 429(3), 2537

Meurer G. R., Obreschkow D., Wong O. I., Zheng Z., Audcent-Ross F. M., Hanish D. J., 2018, MNRAS, 476(2), 1624

Milgrom M., 1983, ApJ, 270, 365

Milgrom M., 2016, arXiv preprint arXiv:1609.06642

Milgrom M., 2016, arXiv preprint arXiv:1610.07538

Navarro J. F., Benitez-Llambay A., Fattahi A., Frenk C. S., Ludlow A. D., Oman K. A., Schaller M., Theuns T., 2017, MNRAS, 471(2), 1841

O'Brien J. C., Freeman K. C., van der Kruit P. C., 2010, A&A, 515, A62

Persic M., Salucci P., 1991, ApJ, 368, 60

Persic M., Salucci P., Stel F., 1996, MNRAS, 281(1), 27

Quirk W. J.,1972, ApJ, 176, L9

Rubin V., Ford W. K. Jr., Thonnard N., 1980, ApJ, 238, 471

Salucci P., Wilkinson M. I., Walker M. G., Gilmore G. F., Grebel E. K., Koch A., Frigerio Martins C., Wyse R. F., 2012, MNRAS, 420(3), 2034

Sanders R. H., 1990, Astronomy & Astrophysics Review, 2(1), 1

Toomre A, 1964, ApJ, 139, 1217

Tully R. B., Fisher J. R., 1977, A&A, 54, 661

van der Kruit P. C., 1981, A&A, 99, 298

van der Kruit P. C., Freeman K. C., 2011, Annual Review of Astronomy and Astrophysics, 49, 301

Wang B., Silk J., 1994, ApJ, 427, 759

Wheeler C., Hopkins P. F., Dore O., 2018, arXiv preprint arXiv:1803.01849

Wong O. I., Meurer G. R., Zheng Z., Heckman T. M., Thilker D. A., Zwaan M. A., 2016, MNRAS, 460(1), 1106

Yegorova I. A., Salucci P., 2007, MNRAS, 337(2), 507

Zheng Z., Meurer G. R., Heckman T. M., Thilker D. A., Zwaan M. A., 2013, MNRAS, 434(4), 3389

Zwicky F., 1937, ApJ, 86, 217